Origin of Rh and Pd agglomeration on the $CeO_2(111)$ surface

Baihai Li,[1,2] Obiefune K. Ezekoye,[2] Qiuju Zhang,[1] Liang Chen,[1,*] Ping Cui,[1] George Graham,[2,*] and Xiaoqing Pan[2,*]
[1]*Institute of Materials Technology and Engineering, Chinese Academy of Sciences, Ningbo 315201, People's Republic of China*
[2]*Department of Materials Science and Engineering, University of Michigan, Ann Arbor, Michigan 48109, USA*
(Received 12 May 2010; revised manuscript received 17 August 2010; published 10 September 2010)

Our theoretical study presents an insight to rationalize the growth behavior of Pd and Rh particles on the $CeO_2(111)$ surface under sequential oxidative and reductive treatments. The oxidation state of Rh atoms plays an important role in the interfacial morphology. Under oxidative conditions, the strong O-Rh-O sandwiched structure inhibits Rh agglomeration. However, the removal of surface oxygen atoms in Rh oxide under reductive conditions facilitates the cleavage of Rh-CeO_2 bonding and consequently results in the agglomeration of metallic Rh. Experimental transmission electron microscopy observations are consistent with the theoretical calculations.

DOI: 10.1103/PhysRevB.82.125422 PACS number(s): 68.35.Fx, 68.35.Ct, 68.37.Og, 71.15.Mb

I. INTRODUCTION

Oxide-supported precious-metal particles have attracted intense interest due to their vast applications in heterogeneous catalysis. Many factors, including the size and distribution of the precious-metal particles, their surface morphology, and defects in the oxides, affect the performance of catalysts during use.[1] Further, operation at high temperature and under harsh atmosphere over long-time inevitably leads to loss of catalytic activity due to damaging effects, such as aggregation of the precious-metal particles. Indeed, effectively controlling the size of precious-metal particles is crucial for maintaining high catalytic activity. The behavior of the metal-oxide interface, which can be quite dynamic, as exemplified by the well-known strong metal-support interaction (SMSI),[2] is of critical importance in this regard.[3–5] This may be of no greater significance than in the three-way catalyst (TWC), which consists of a complex mixture of precious-metal particles (Pt, Pd, and Rh) and oxide materials, and provides the most effective approach to mitigating harmful gaseous emissions, such as CO, NO_x, and unburned hydrocarbons, from gasoline engines worldwide. CeO_2 is perhaps the most important oxide ingredient in the TWC because of its well-known oxygen-storage capacity,[6–9] and the behavior of precious-metal particles supported on the CeO_2 surface has been studied extensively.[10,11]

A clear understanding of the nucleation and growth of metal particles on the oxide support is certainly of importance for controlling the catalyst particle size and preventing unwanted agglomeration. However, due to the complexity of the interfaces, it is hard to achieve a fundamental understanding of the underlying mechanisms by experimental study alone, whereas computational approaches can provide a picture of the detailed nature of metal-support interactions.[12,13] For example, the static adhesion of precious metals (atoms and monolayer) on the $CeO_2(111)$ surface has been widely studied by means of DFT+U methods.[14] It was found that the metal-support interactions are mainly of an electrostatic nature, and the structures and electronic properties of the interface are sensitive to the binding site and oxygen coordination of the metal atoms.[14–16] Aside from the reported energetics, however, data on the kinetics, which are required to predict and rationalize the growth mode of the metal particles on the oxide support,[17] are largely absent. In the present work, we carried out comparative studies on the diffusion and clustering of Pd and Rh atoms on $CeO_2(111)$ by using density-functional methods, and we contrast our results with high-resolution transmission electron microscopy (HRTEM) observations. Our goal is to understand the evolution of the metal-support interface at the atomistic scale, as well as some aspects of SMSI in heterogeneous catalysis.

II. METHODOLOGY

A. Computational methods

Spin-polarized DFT+U calculations were performed using the Vienna *ab initio* simulation package (VASP).[18] The value of U_{eff} was set to 5 eV as suggested in many theoretical works.[14,19–21] The electron exchange and correlation were treated within the generalized gradient approximation using the Perdew-Burke-Ernzerhof functional.[22] The projector-augmented-wave method[23] was used for the treatment of the core electrons. The 5*s*, 5*p*, 5*d*, 4*f*, and 6*s* electrons of Ce, the 2*s* and 2*p* electrons of O, the 4*d* and 5*s* electrons of Pd and Rh were treated as valence electrons. All atoms were fully relaxed with the forces converged to less than 0.03 eV/Å. Electron smearing was employed using the Methfessel-Paxton technique,[24] with a smearing width of $\sigma = 0.1$ eV, in order to minimize the errors in the Hellmann-Feynman forces. The nudged elastic band (NEB) (Ref. 25) method was used to examine the energy profiles along selected diffusion pathways. Electron transfers were analyzed based on the Bader partitioning scheme.[26]

Ceria is a rare-earth oxide in cubic fluorite structure with four Ce atoms and eight O atoms per unit cell. Our calculated lattice parameter is 5.44 Å, which agrees very well with the experimental value of 5.41 Å (Ref. 27) and other reported theoretical results.[14,28] The nonpolar $CeO_2(111)$ surface, the structurally most close-packed, is found to be the energetically most stable surface. Gennard *et al.*[29] have shown that a slab containing nine $CeO_2(111)$ layers is sufficient to converge the important surface properties including surface energy, Mulliken charges and electron densities.

Therefore, to study the energetics and electronic structures of single atoms on the CeO_2 substrate, we built a (2×2) supercell containing nine sandwiched O-Ce-O layers and 14 Å vacuum space. The $3\times3\times1$ Monkhorst-Pack mesh[30] was used to sample the Brillouin zone. Our calculated surface energy is 0.039 $eV/Å^2$, which is consistent with other theoretical results (0.037–0.042 $eV/Å^2$).[28,31] For the Pd_{13} and Rh_{13} clusters on $CeO_2(111)$ and *ab initio* molecular-dynamics (MD) simulations, we adopted a larger (3×3) supercell in order to avoid lateral interactions of the clusters between images.

B. Experimental approach

Thick (~150 nm) CeO_2 films were grown on the (111) surface of yttria-stabilized zirconia (YSZ) using pulsed laser deposition (PLD) in an on-axis geometry. The PLD system was equipped with a 248 nm KrF laser (Compex 205, Lambda-Physik) with nominal pulse width of 22 ns. The substrates were heated during deposition using a radiatively heated substrate stage. The CeO_2 target was sintered from commercial CeO_2 powder. The substrate-to-target distance was approximately 6.5 cm. Deposition parameters were optimized for both crystalline quality and surface finish, measured by x-ray diffraction (XRD) (Rigaku) and atomic force microscopy (AFM) (Digital Instruments Nanoscope IIIa), respectively. Growth conditions for the CeO_2 films were as follows: substrate temperature of 1073 K, laser energy of 100 mJ, laser repetition rate of 5 Hz, and an oxygen partial pressure of 6 mTorr. The CeO_2 films were heated in air for 1 h at 873 K after their deposition onto the YSZ substrates and the samples were then placed in an ultrahigh vacuum (UHV) chamber (Physical Electronics Industries), described in detail previously,[32] and a monolayer equivalent of metal (either Pd or Rh) was deposited using a thermal evaporation source. Metal coverage was monitored using x-ray photoelectron spectroscopy (XPS). After deposition, the samples were subjected to various thermal treatments, as described in Sec. III D below. Cross-section TEM specimens were thinned to electron transparency using traditional methods of mechanical grinding and argon ion milling using an accelerating voltage of 4 kV at an angle of 3.7°–4.2° (Gatan model 691 precision ion polishing system). TEM studies were carried out on a JEOL 3011 high-resolution electron microscope operated at 300 kV with a point-to-point resolution of 0.17 nm.

III. RESULTS AND DISCUSSION

A. Pd and Rh clusters on $CeO_2(111)$

For the metal/oxide interface, the geometric and electronic structures are directly associated with their catalytic properties and have thus attracted particular interest. The adhesion of noble metal atoms or monolayers on $CeO_2(111)$ has been extensively investigated. To avoid redundancy, we only include our calculated energetics of Rh and Pd atoms and monolayers on $CeO_2(111)$ in the supplementary material.[33] In general, our calculations are in good agreement with previous studies.[14,15,21] The sequence of the binding strength is as following: Rh-Rh > Pd-Pd > Rh-CeO_2 > Pd-CeO_2. In this section, we will instead focus on the metal clusters on $CeO_2(111)$. In fact, whether or not adatoms can form clusters on the substrate depends on a delicate balance between the adatom-substrate and adatom-adatom lateral interactions.[34,35] In principle, if the metal-substrate interactions are strong enough to dominate over the metal-metal lateral interactions, the metal tends to form two-dimensional (2D) layer structures. To carefully compare the adatom-adatom and adatom-substrate interactions and thus evaluate the relative stability of the clusters on the substrate, we first chose the smallest three-dimensional (3D) Pd_4 and Rh_4 tetrahedron clusters and placed them in sufficiently large boxes to calculate their cohesive energies. Subsequently, we placed them on the CeO_2 substrate to calculate the adhesion energies, as displayed in the left panel of Fig. 1. The calculated cohesive energies for Pd_4 and Rh_4 are 1.69 eV/atom and 2.62 eV/atom, respectively. Structural optimizations of $Pd_4/CeO_2(111)$ and $Rh_4/CeO_2(111)$ show that the structures of the adsorbed Pd_4 and Rh_4 clusters as well as the substrate surface are only slightly distorted. The three bottom atoms of Pd_4 and Rh_4 clusters reside above three adjacent surface oxygen atoms, forming three tilted bonds with the bond lengths of 2.07 Å for Pd-O, and 2.01 Å for Rh-O, respectively. The top Pd and Rh atoms gains 0.15 and 0.19 electrons from the three bottom atoms while each bottom Pd and Rh atom donates 0.13 and 0.24 electrons to the substrate and the upper atom, respectively. As a result, the Pd_4 and Rh_4 clusters become slightly polarized. Certainly, such charge transfer should lead to different catalytic performance from the unsupported Pd_4 and Rh_4 clusters (or clusters supported on an inert oxide, such as Al_2O_3). The total binding energy for Pd_4 and Rh_4 on $CeO_2(111)$ are calculated to be 2.48 eV/atom and 3.73 eV/atom, which are 0.54 eV and 0.83 eV larger than those of Pd and Rh monolayers deposited on $CeO_2(111)$, respectively.[33]

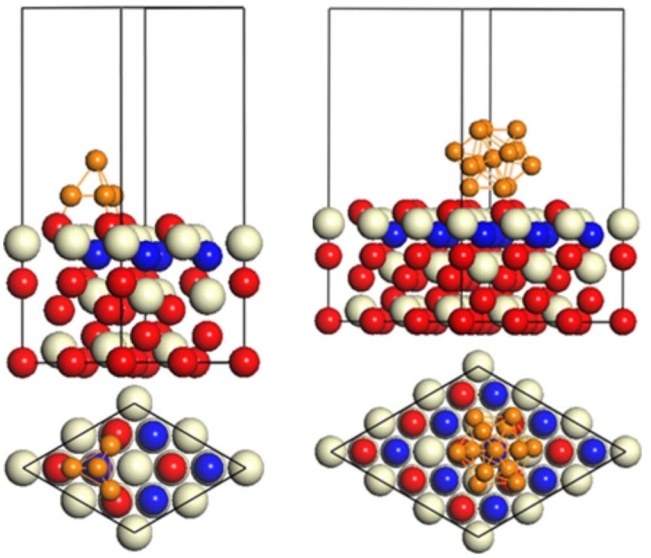

FIG. 1. (Color online) Deposition of Pd_4,(Rh_4) (left panel) and $Pd_{13}(Rh_{13})$ (right panel) clusters on $CeO_2(111)$: (top) Side views; (bottom) top views. The orange and white spheres represent Pd(or Rh) and Ce atoms, respectively. The subsurface O atoms (O_S) are highlighted as blue spheres while the surface O atoms (O_F) and other O atoms are represented as red spheres.

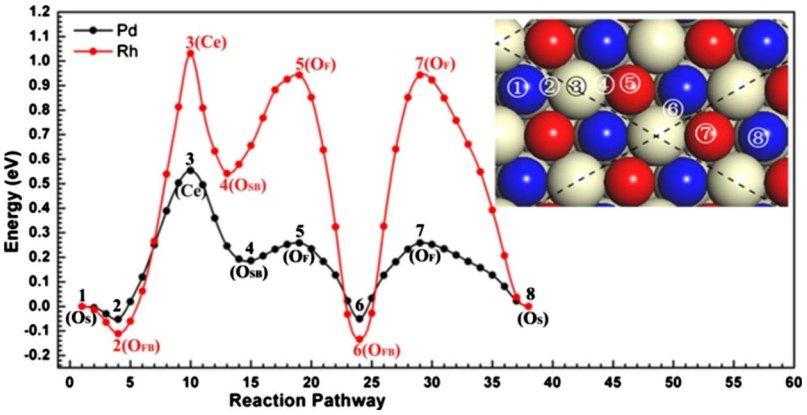

FIG. 2. (Color online) The energy profiles of the single Pd and Rh atoms migration on $CeO_2(111)$. All the energies are compared to Pd and Rh deposited on the O_S site, respectively. The specified diffusion pathway is noted on the inserted slice.

The Pd_4 and Rh_4 clusters are the smallest possible 3D clusters. To better model realistic clusters under our computational limitation, we next chose larger icosahedral Pd_{13} and Rh_{13} clusters with diameters of around 0.80 nm and calculated their cohesive energies as well as the cluster-substrate adhesion energies. It is found that Pd_{13} and Rh_{13} clusters prefer to adopt an orientation with one (111) facet interacting with the $CeO_2(111)$ surface, as shown in the right panel of Fig. 1. There is very little distortion for Pd_{13} and Rh_{13} clusters, of which the bottom plane locates above three outmost O_F ions forming three equivalent Pd-O_F and Rh-O_F bonds of 2.03 Å for $Pd_{13}/CeO_2(111)$ and 1.98 Å for $Rh_{13}/CeO_2(111)$, respectively. The calculated cohesive energies for the isolated Pd_{13} and Rh_{13} clusters are 2.32 eV/atom and 3.63 eV/atom, respectively, which are 0.7–1.0 eV stronger than in the isolated tetrahedral clusters. Indeed, the lower coordination number in the tetrahedral clusters greatly reduces their cohesive energies. By comparing the adhesion energy with the cohesive energy, it is demonstrated again that metal-metal interactions are much stronger than metal-substrate interactions. Ideally, Pd and Rh prefer to form clusters on the substrate.

B. Transition of Pd and Rh monolayers to clusters on $CeO_2(111)$

On the basis of the calculations above, the agglomeration of Pd and Rh atoms on $CeO_2(111)$ appears to be inevitable since 3D particles are more favorable than the 2D layers in terms of thermodynamics. However, the transition from the 2D layer to 3D particles might be hindered by some kinetic factors so that it can only occur if Pd and Rh atoms gain sufficient kinetic energy to overcome activation barriers at elevated temperatures. In order to adequately understand the underlying kinetics, we performed NEB calculations to map out the energy profiles along some prescribed pathways. First of all, evaluation of the mobility of Pd or Rh atoms on $CeO_2(111)$ is critical because the clustering process at low coverage certainly involves single atom diffusion. The energy profiles of Pd and Rh atoms migration on the $CeO_2(111)$ surface are shown in Fig. 2. Here we selected a rounded path to sample all the possible hopping routes between each high-symmetry binding site. NEB calculations indicate that there is no evident activation barrier for each hopping step, i.e., the energy curves between each state are monotonically increasing or decreasing. The frequency calculations confirmed that each state is stable (not a transition state). Along the entire migration pathway, the Ce site (state 3) is the most unfavorable binding site, where Pd and Rh diffusion from the O_{FB} site see the highest barrier of 0.62 eV and 1.16 eV, respectively. Nevertheless, the moderate activation barriers (<0.25 eV) indicate that the diffusion of Pd atoms on $CeO_2(111)$, excluding the Ce site, could be facile even at moderate temperatures. In contrast, Rh exhibits much lower mobility. It is very likely that Rh atoms are trapped and frozen at some specific sites.

The transition from the planar overlayer to a tetrahedral cluster can clearly reflect how the metal-O bonds are cleaved because of the strong metal-metal cohesive energy. Furthermore, it may serve as the key step for the subsequent nucleation and particle growth. Herein we propose a concerted mechanism that involves the motion of multiple Pd (or Rh) atoms simultaneously. In light of previous studies,[15,34,36] we found that one monolayer of Pd or Rh atoms on the O_F sites is energetically the most stable and thus chose them as the initial state for the following NEB calculations. As depicted in the insets of Fig. 3, one Pd (or Rh) atom at the site A moves toward the other Pd (or Rh) atom at the site B. Consequently, the Pd (or Rh) atom originally at the site B is

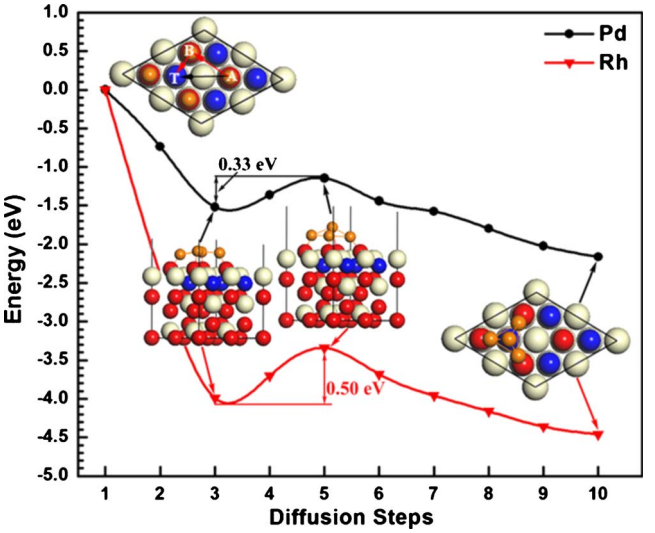

FIG. 3. (Color online) Energy profiles of the Pd and Rh transitions from 2D layer to tetrahedral clusters on $CeO_2(111)$.

pushed onto the site T above the Pd (or Rh) layer. For comparison, we have also considered an alternative mechanism in which one Pd or Rh atom hops directly from the site A onto the top of the triangle. However, such a mechanism seems unfavorable because of the considerably higher activation barrier.

In this concerted mechanism, both Pd and Rh behave quite similarly: all atoms in the overlayer first get closer in the plane and gradually evolve to the intermediate 2D "island" (state-II in Fig. 3) with shorter Pd-Pd (2.67–2.75 Å) and Rh-Rh (2.42–2.63 Å) bond lengths. This step is barrierless due to the reduced coordination numbers of the atoms (compared to bulk) and high in-plane mobility of Pd and Rh atoms on $CeO_2(111)$. Indeed, the subsequent molecular dynamics simulations confirmed that this step can occur very easily. The state-III is identified as the transition state with energy barriers of 0.33 eV and 0.5 eV for Pd and Rh, respectively. The barrier mainly arises from the breaking of Pd-O and Rh-O bonds. The Pd and Rh atoms originally at the site B are lifted from the surface plane, and the corresponding Pd-O and Rh-O bonds are elongated by approximately 1.0 Å. Rh has higher cohesive energy than Pd, implying that Rh can form a cluster more easily than Pd, at least thermodynamically. However, kinetic factors slow down the agglomeration.

C. Molecular-dynamics simulations

The calculations above suggested that there is a greater tendency for Pd to agglomerate into 3D particles on $CeO_2(111)$ than Rh. Unfortunately, the NEB calculations neglect the motion of surface oxygen atoms, which actually plays a critical role in the realistic clustering process and also requires some activation energy. Hence, the activation barrier for the 2D-3D transition is underestimated in the NEB calculations. Indeed, noble metals have been shown to significantly enhance the oxygen storage/release capability of CeO_2.[14,37–39] Thus, the mobility of oxygen atoms is also important and must be considered in the presence of the Pd and Rh overlayers. In this regard, we next performed *ab initio* MD simulations at varying temperatures (300–1200 K) within the canonical *NVT* ensemble to simulate the clustering process. In the initial state, one monolayer of metal atoms was placed on ceria with each metal atom on its most stable binding site, which is identical to the initial structure in the prior NEB simulation. At temperatures lower than 900 K, no clustering behavior of Pd atoms was observed in the MD simulations for up to 5 ps, although they moved closer to form 2D islands. The upper panel of Fig. 4 displays the evolution of the Pd layer on $CeO_2(111)$ at 900 K. After 2.5 ps, the formation of a tetrahedron was observed. One Pd atom gains enough kinetic energy and is able to pass the barrier for the 2D-3D transition. After another 0.5 ps, the tetrahedron cluster remains nearly intact.

In contrast, no formation of 3D Rh clusters is detected in the entire MD simulations at up to 1200 K. In principle, Rh atoms are still able to agglomerate at sufficiently high temperatures due to the strong cohesive energy. However, the $CeO_2(111)$ surface has limited thermodynamic stability and

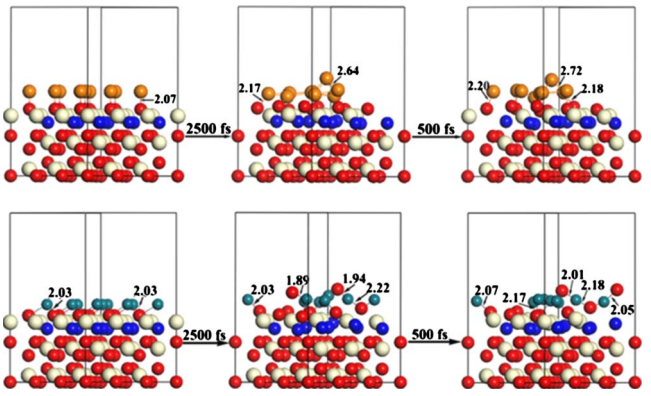

FIG. 4. (Color online) Simulation snapshots for the evolution of $Pd/CeO_2(111)$ interface at 900 K (upper panel) and the evolution of $Rh/CeO_2(111)$ interface at 1200 K (lower panel). The highlighted bond lengths of Pd(Rh)-O are in the unit of Å. The orange and dark blue spheres represent Pd and Rh atoms, respectively.

tends to lose oxygen upon heating. As illustrated in the lower panel of Fig. 4, some surface oxygen atoms are desorbed from the $CeO_2(111)$ surface plane and diffuse onto the Rh layer at 1200 K. Naturally, this atomic oxygen (denoted as O_{upper}, whereas the oxygen in CeO_2 will be denoted as O_{ceria}) is extremely reactive and able to oxidize Rh to RhO_x. The corresponding Rh-O_{upper} bond lengths are calculated to be 1.9–2.1 Å, which is in line with the bond lengths of the crystalline Rh_2O_3. In the following 3 ps of simulation, the RhO_x layer persists. Because of the highly reactive nature of O_{upper}, the Rh-O_{upper} bonding strength (5.27 eV) is much greater than either Rh-Rh cohesive (3.24 eV) or Rh-O_{ceria} adhesive energy (2.90 eV). Thus, the stable O_{upper}-Rh-O_{ceria} sandwich structure is formed. In fact, similar structures have been observed on the PtO-Al_2O_3 interfaces very recently.[5] In actual use, the TWC usually undergoes repeated reduction and oxidation treatment. The oxidation and reduction treatments are believed to play different roles in the growth and dispersion of metal particles.[40,41] Specifically, oxidation can reverse the effects of sintering and redisperse the metal particles on the ceria-based oxide surface.[41] Indeed, the formation of RhO_x and the strong O_{upper}-Rh-O_{ceria} bonds would hinder or prevent the coalescence of 3D metallic Rh particles.

In order to ascertain the influence of a reduction treatment, we next investigated the evolution of a Rh overlayer on a prereduced $CeO_2(111)$ surface. 30% of the surface O_{ceria} atoms were directly removed to mimic the exhaust gas system under the severely reduced atmosphere. Note that the oxygen vacancies are found to be neutral, which has been experimentally confirmed at oxygen deficient conditions.[42] The MD simulations performed at 900 and 1200 K indicate that the dynamics are similar to those on the unreduced CeO_2 surface. Rh atoms aggregate to form 2D islands. At the same time, some oxygen atoms move out of the surface plane and diffuse onto the Rh overlayer forming Rh oxide (the upper panel of Fig. 5). The insensitivity of these results to the removal of the surface O_{ceria} atoms is consistent with the recent STM observation that the oxidation state of the ceria substrate does not cause an observable change in the growth of Rh or Pd overlayers.[17]

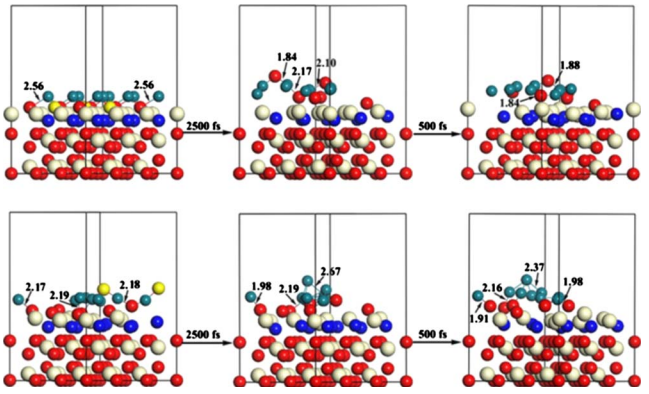

FIG. 5. (Color online) Simulation snapshots for the evolution of Rh overlayer on the reduced $CeO_2(111)$ surface (upper panel) and reduced Rh oxide on the $CeO_2(111)$ surface at 1200 K (lower panel). The yellow spheres represent the removed oxygen atoms to mimic the reduction treatment. The highlighted bond lengths of Rh-O are in the unit of Å.

On the other hand, we also considered the reduction in both the CeO_2 substrate and the Rh oxide that formed in the 1200 K simulation. That is, we chose the final structure of Rh/CeO_2 simulated at 1200 K and removed the two oxygen atoms that diffused onto the Rh layer. As shown in the lower panel of Fig. 5, the subsequent dynamics turn out to be strikingly different. The metallic Rh atoms from reduced RhO_x form 3D clusters rapidly, within 1–1.5 ps. After another 2 ps, only the shape of the clusters undergoes change. We also observed that the 3D clusters can form at even lower temperature (900 K), following reduction in RhO_x. On the basis of the two simulations above, we can conclude that the agglomeration of Rh is influenced more by the oxidation state of Rh than the ceria surface. Careful analysis of the two starting structures reveals a subtle but critical difference. For the reduced Rh oxide (metallic Rh), the O_{upper} atoms that originally resided above the Rh layers become the driving force to pull the Rh atoms from the CeO_2 surface by forming strong Rh-O_{upper} bonds. Obviously, this driving force partially offset the activation energies required for breaking the Rh-O_{ceria} bonds by lifting the Rh atoms closer to the transition state. Indeed, the associated Rh-O_{ceria} bonds are elongated by approximately 0.1 Å. In the reduction process, removal of the O_{upper} atoms would leave these lifted Rh atoms rather "mobile" and able to readily hop onto the Rh layer. Consequently, the formation of metallic Rh clusters becomes much more facile. In contrast, the reduction of the CeO_2 substrate cannot solely facilitate the agglomeration of Rh since the competitive driving force from the O_{upper} atoms is absent.

D. TEM experiments

To lend support to the theoretical results above, we also performed experiments. As described in Sec. II B, a monolayer equivalent of metal (either Pd or Rh) was thermally evaporated onto a $CeO_2(111)$ film [150-nm-thick, previously grown on (111) yttria-stabilized zirconia substrates] in UHV. Typical analytical results characterizing the $CeO_2(111)$ film

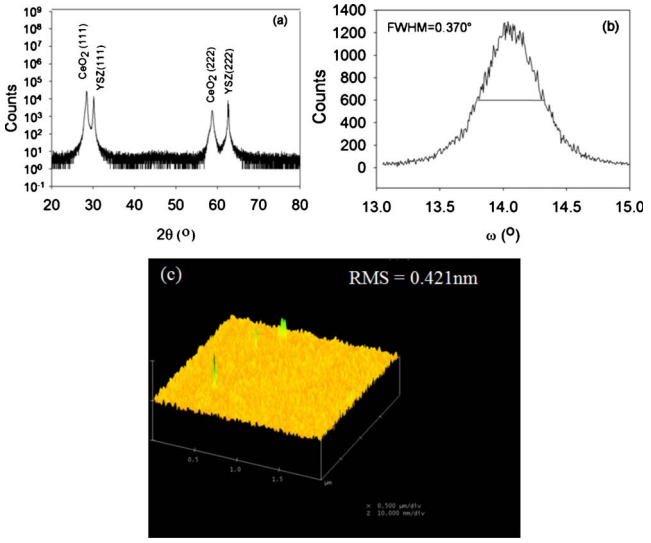

FIG. 6. (Color online) (a) $\theta/2\theta$ XRD of CeO_2 on YSZ(111) (b) ω-rocking curve of CeO_2 111 peak, and (c) 2 μm$\times$2 μm AFM surface plot of CeO_2/YSZ film.

and the Pd monolayer, for example, are shown in Figs. 6 and 7, respectively. The $\theta/2\theta$ measurement in Fig. 6(a) confirms that the ceria film is single crystalline with no major contributions from secondary phases. Furthermore, the $\theta/2\theta$ scan indicates that the CeO_2 film is in an epitaxial relationship with the YSZ (111) substrate. The ω scan in Fig. 6(b), where the full width at half maximum of the $CeO_2(111)$ peak is 0.370°, indicates a high crystalline quality, considering that the film thickness is ~150 nm. The AFM result, Fig. 6(c), establishes that the film surface is relatively flat and smooth. The XPS results in Fig. 7 provide assurance that the surface composition before and after Pd deposition is as expected. We note that the negligible attenuation of ceria signal by Pd implies that a significant degree of Pd agglomeration actually took place upon deposition.

After metal deposition, the films were calcined in air for 1 h at 873 K and cross-sectional specimens were prepared for TEM examination. The TEM image of the surface of the

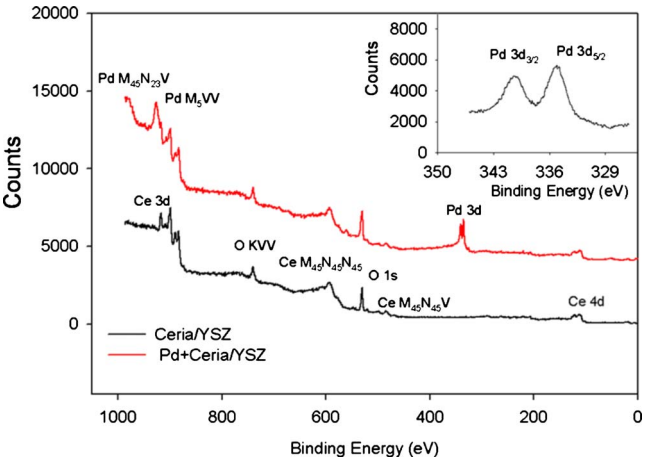

FIG. 7. (Color online) XPS spectra of CeO_2/YSZ film (before and after Pd deposition). Insert shows detail of the Pd-3D spectrum.

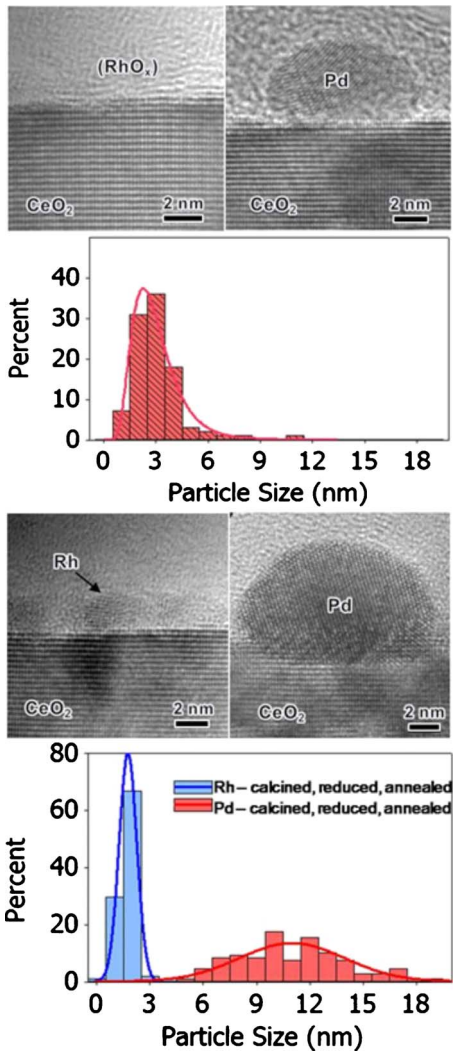

FIG. 8. (Color online) Histograms and HRTEM images of Pd and Rh particles on the $CeO_2(111)$ surface following calcination (top) and calcination/reduction/annealing (bottom) treatments (see text for details).

CeO_2 film with Pd clearly reveals Pd-derived (according to energy dispersive spectroscopy) particles on the ceria surface. As observed previously, these particles, which are initially Pd oxide, decompose into Pd metal relatively quickly under the influence of the electron beam in the TEM.[42] The diameters of 100 particles were measured, and the corresponding histogram is presented in the upper half of Fig. 8. The mean particle size was calculated to be 3 nm. A HRTEM image of one of the resulting Pd metal particles is shown in the upper right half of Fig. 8. In contrast, there was no evidence of Rh-derived particles on the surface of the CeO_2 film with Rh (upper left half of Fig. 8). We conclude that the Rh-derived particle size is too small to be resolvable in our HRTEM. As in the case of Pd, the stable form of Rh under this treatment condition (873 K in air) would be its oxide.

Our assumption is that some degree of particle coarsening could occur before these oxides form, after which the particles may be expected to remain relatively stable. There is evidence that Rh may react with ceria[11] and the kinetics of oxide formation are presumably different between Pd and Rh so that the oxides are likely to form at different temperatures. These considerations notwithstanding, the HRTEM observations demonstrate more facile formation of Pd than Rh particles on $CeO_2(111)$.

We also subjected both calcined films to a brief reduction treatment (20 min in flowing nitrogen containing 1% H_2 at 473 K), in order to convert any Pd or Rh oxides to metals, followed by a long annealing treatment (5 h in flowing nitrogen at 973 K). The reduction and annealing treatments were then repeated, and TEM specimens were prepared. In this case, small metallic Rh particles with mean particle size of 2.2 nm were clearly observed, while the Pd particles, now metallic from the outset, were found to be even larger, with mean particle size of 11 nm (lower half of Fig. 8). Therefore, reduction in the metal oxides on the support can further facilitate the agglomeration of both metal particles.

IV. CONCLUSIONS

In summary, we show that Pd and Rh 3D particles are energetically preferred (relative to isolated atoms and 2D islands) on the $CeO_2(111)$ surface due to the strong cohesive energy. Kinetically, Pd exhibits greater tendency to agglomerate into 3D particles than Rh. The further MD simulations present an insight to rationalize the growth behavior of Rh particles on the $CeO_2(111)$ surface under sequential oxidative and reductive treatments. The oxidation state of Rh atoms is found to play an important role in the interfacial morphology. Under oxidative conditions, the strong Rh-O interactions inhibit Rh agglomeration. However, the removal of surface oxygen atoms in Rh oxide under reductive conditions facilitates the cleavage in Rh-CeO_2 bonding and consequently results in the agglomeration of metallic Rh. Experimental TEM observations are consistent with our theoretical calculations.

ACKNOWLEDGMENTS

Electron microscopy studies at the Electron Microbeam Analysis Laboratory at the University of Michigan were supported by the National Science Foundation under Grant No. DMR-0315633. We gratefully thank the financial support from innovative project of Chinese academy of sciences, Ningbo municipal government, and Ningbo science foundation.

*Author to whom correspondence should be addressed.

[1] M. Valden, X. Lai, and D. W. Goodman, Science **281**, 1647 (1998).
[2] S. J. Tauster, Acc. Chem. Res. **20**, 389 (1987).
[3] X. Q. Gong, A. Selloni, O. Dulub, P. Jacobson, and U. Diebold, J. Am. Chem. Soc. **130**, 370 (2008).
[4] M. Sterrer, T. Risse, L. Giordano, M. Heyde, N. Nilius, H. P. Rust, G. Pacchioni, and H. J. Freund, Angew. Chem., Int. Ed. **46**, 8703 (2007).
[5] J. H. Kwak, J. Z. Hu, D. Mei, C. W. Yi, D. H. Kim, C. H. F. Peden, L. F. Allard, and J. Szanyi, Science **325**, 1670 (2009).
[6] M. V. Ganduglia-Pirovano, A. Hofmann, and J. Sauer, Surf. Sci. Rep. **62**, 219 (2007).
[7] N. V. Skorodumova, S. I. Simak, B. I. Lundqvist, I. A. Abrikosov, and B. Johansson, Phys. Rev. Lett. **89**, 166601 (2002).
[8] S. D. Park, J. M. Vohs, and R. J. Gorte, Nature (London) **404**, 265 (2000).
[9] Q. Fu, H. Saltsburg, and M. Flytzani-Stephanopoulos, Science **301**, 935 (2003).
[10] H. Cordatos and R. J. Gorte, J. Catal. **159**, 112 (1996).
[11] S. Imamura, T. Yamashita, R. Hamada, Y. Saito, Y. Nakao, N. Tsuda, and C. Kaito, J. Mol. Catal. Chem. **129**, 249 (1998).
[12] L. Giordano, C. Di Valentin, J. Goniakowski, and G. Pacchioni, Phys. Rev. Lett. **92**, 096105 (2004).
[13] M. A. San-Miguel, J. Oviedo, and J. F. Sanz, Phys. Rev. Lett. **99**, 066102 (2007).
[14] Z. X. Yang, Z. S. Lu, and G. X. Luo, Phys. Rev. B **76**, 075421 (2007).
[15] M. Alfredsson and C. R. A. Catlow, Phys. Chem. Chem. Phys. **4**, 6100 (2002).
[16] E. L. Wilson, R. Grau-Crespo, C. L. Pang, G. Cabailh, Q. Chen, J. A. Purton, C. R. A. Catlow, W. A. Brown, N. H. de Leeuw, and G. Thornton, J. Phys. Chem. C **112**, 10918 (2008).
[17] J. Zhou, A. P. Baddorf, D. R. Mullins, and S. H. Overbury, J. Phys. Chem. C **112**, 9336 (2008).
[18] G. Kresse and J. Hafner, Phys. Rev. B **48**, 13115 (1993).
[19] M. Nolan, S. C. Parker, and G. W. Watson, Surf. Sci. **595**, 223 (2005).
[20] D. Knapp and T. Ziegler, J. Phys. Chem. C **112**, 17311 (2008).
[21] Z. Yang, L. A. Zhansheng, G. Luo, and K. Hermansson, Phys. Lett. A **369**, 132 (2007).
[22] J. P. Perdew, J. A. Chevary, S. H. Vosko, K. A. Jackson, M. R. Pederson, D. J. Singh, and C. Fiolhais, Phys. Rev. B **46**, 6671 (1992).
[23] P. E. Blöchl, Phys. Rev. B **50**, 17953 (1994).
[24] M. Methfessel and A. T. Paxton, Phys. Rev. B **40**, 3616 (1989).
[25] G. Henkelman, B. P. Uberuaga, and P. Jonsson, J. Chem. Phys. **113**, 9901 (2000).
[26] R. F. W. Bader, *Atoms in Molecules: A Quantum Theory* (Oxford University Press, New York, 1990).
[27] H. J. Whitfield, D. Roman, and A. R. Palmer, J. Inorg. Nucl. Chem. **28**, 2817 (1966).
[28] S. Kumar and P. K. Schelling, J. Chem. Phys. **125**, 204704 (2006).
[29] S. Gennard, F. Cora, and C. R. A. Catlow, J. Phys. Chem. B **103**, 10158 (1999).
[30] H. J. Monkhorst and J. D. Pack, Phys. Rev. B **13**, 5188 (1976).
[31] Z. X. Yang, T. K. Woo, M. Baudin, and K. Hermansson, J. Chem. Phys. **120**, 7741 (2004).
[32] G. W. Graham, Surf. Sci. **268**, 25 (1992).
[33] See supplementary material at http://link.aps.org/supplemental/10.1103/PhysRevB.82.125422 for the calculated energetics and electronic structures of Pd and Rh single atoms and monolayers on CeO_2(111).
[34] M. Alfredsson and C. R. A. Catlow, Surf. Sci. **561**, 43 (2004).
[35] L. Chen and J. K. Johnson, Phys. Rev. Lett. **94**, 125701 (2005).
[36] M. Alfredsson and C. R. A. Catlow, Phys. Chem. Chem. Phys. **3**, 4129 (2001).
[37] H. C. Yao and Y. F. Y. Yao, J. Catal. **86**, 254 (1984).
[38] H. Cordatos, T. Bunluesin, J. Stubenrauch, J. M. Vohs, and R. J. Gorte, J. Phys. Chem. **100**, 785 (1996).
[39] C. J. Weststrate, R. Westerstrom, E. Lundgren, A. Mikkelsen, and J. N. Andersen, J. Phys. Chem. C **113**, 724 (2009).
[40] Y. Nagai, K. Dohmae, Y. Ikeda, N. Takagi, T. Tanabe, N. Hara, G. Guilera, S. Pascarelli, M. A. Newton, O. Kuno, H. Jiang, H. Shinjoh, and S. Matsumoto, Angew. Chem., Int. Ed. **47**, 9303 (2008).
[41] M. Hatanaka, N. Takahashi, T. Tanabe, Y. Nagai, A. Suda, and H. Shinjoh, J. Catal. **266**, 182 (2009).
[42] Y. Jiang, J. B. Adams, M. van Schilfgaarde, R. Sharma, and P. A. Crozier, Appl. Phys. Lett. **87**, 141917 (2005).